Biochemistry

 Volume 42, Number 14 April 15, 2003

Articles

Rational Design of Genetically Encoded Fluorescence Resonance Energy Transfer-Based Sensors of Cellular Cdc42 Signaling†

Abhinav Seth,‡ Takanori Otomo,‡ Helen L. Yin,§ and Michael K. Rosen*,‡

Departments of Biochemistry, Pharmacology, and Physiology, University of Texas Southwestern Medical Center, 5323 Harry Hines Boulevard, Dallas, Texas 75390

Received September 20, 2002; Revised Manuscript Received January 13, 2003

ABSTRACT: The temporal and spatial control of Rho GTPase signaling pathways is a central issue in understanding the molecular mechanisms that generate complex cellular movements. The Rho protein Cdc42 induces a significant conformational change in its downstream effector, the Wiskott−Aldrich syndrome protein (WASP). On the basis of this conformational change, we have created a series of single-molecule sensors for both active Cdc42 and Cdc42 guanine nucleotide exchange factors (GEFs) that utilize fluorescence resonance energy transfer (FRET) between cyan and yellow fluorescent proteins. In vitro, the Cdc42 sensors produce up to 3.2-fold FRET emission ratio changes upon binding active Cdc42. The GEF sensors yield up to 1.7-fold changes in FRET upon exchange of GDP for GTP. The GEF-catalyzed rate of nucleotide exchange for the GEF sensor is indistinguishable from that of wild-type Cdc42, but GAP-catalyzed nucleotide hydrolysis is slowed approximately 16-fold. In vivo, both sensors faithfully report on Cdc42 and/or Cdc42-GEF activity. These results establish the successful creation of rationally designed and genetically encoded tools that can be used to image the activity of biologically and medically important molecules in living systems.

Cellular signal transduction relies on dynamically regulated networks of signaling pathways. Correct intracellular localization of individual molecules is essential for precise, specific, and efficient transfer of information along those pathways (*1*). Temporal regulation of activated signaling molecules must also be achieved if multiple signals are to be properly integrated (*2*). To understand how cells maintain the fidelity of signal transduction, it is essential to study signaling processes within a cellular context.

Members of the Rho subfamily of small GTPases have effects on multiple cellular functions including cell migration, proliferation, and gene expression (*3*). To date, most studies of this family have focused on three proteins, Rho, Rac, and Cdc42, and their ability to regulate the actin cytoskeleton (*4*). Like other members of the Ras superfamily, the Rho proteins act as membrane-localized molecular switches, which cycle between active GTP-bound states and inactive GDP-bound states. The intrinsic rates of nucleotide hydrolysis and exchange are slow, and in vivo these processes are controlled by regulatory molecules that accelerate individual steps of the GTPase cycle (*5*). The Dbl family of guanine nucleotide exchange factors (GEFs)[1] activates the Rho

† This work was supported by NIH Grants GM56322 (M.K.R.), GM51112 (H.L.Y.), and GM61203 (H.L.Y.) and Robert A. Welch Foundation Grant I1544 (M.K.R.). T.O. is supported by the Human Frontier Science Program. A.S. is supported by the MST Program and the Division of Cell and Molecular Biology at UT Southwestern.

* Corresponding author. Tel: (214) 648-4703. Fax: (214) 648-8856. E-mail: mrosen@biochem.swmed.edu.

‡ Departments of Biochemistry and Pharmacology.

§ Department of Physiology.

10.1021/bi026881z CCC: $25.00
Published on Web 03/18/2003

GTPases by facilitating release of bound GDP, which results in GTP loading in vivo (*6*). GTPase activating proteins (GAPs) inactivate the Rho proteins by enhancing their intrinsic GTPase activity. Guanine nucleotide dissociation inhibitors (GDIs) inhibit Rho GTPases by sequestering them in the cytosol and by preventing dissociation of bound nucleotide. To date, many GAPs, GDIs, and GEFs have been described with varying selectivity for the different Rho proteins (*3*).

Cdc42 has specific effects on cell motility, intracellular trafficking, establishment and maintenance of cell polarity, and RNA processing (*7*). Cdc42 mediates many of these effects through GTP-dependent interactions with effector proteins containing a Cdc42/Rac interactive binding (CRIB) motif (*8*, *9*). The specific biological consequences of Cdc42 activation are dictated by the subset of effectors, and the degree to which each is activated, in response to a particular signal. Recent data suggest that effector choice depends greatly on the localization of activated GTPase (*10*−*12*). Thus, different cellular pools of Cdc42 may be selectively activated to regulate different cellular functions, but it has not been established which pools are associated with which functions. In addition, the mechanisms by which localized GTPase signals are generated are not well understood (*13*). Attempts to study this aspect of Cdc42 biology have been difficult because of the lack of tools for determining the precise subcellular localization of activated GTPases (as distinct from the total pool) in a living cell.

Despite the existing limitations, efforts have been made to understand the spatial and temporal aspects of Cdc42 signaling using anti-Cdc42 antibodies, mutant GTPases, and chimeras of Cdc42 and green fluorescent protein (GFP). In the absence of stimulation, Cdc42 resides on nuclear, endoplasmic reticulum and Golgi membranes as well as in the cytoplasm, presumably bound to RhoGDI (*14*−*16*). Cdc42 also localizes to podosomes, actin-rich adhesion structures specific to macrophages (*17*). During Fc γ receptor (FcγR) mediated phagocytosis, a Cdc42-dependent process, the GTPase accumulates at phagosome sites along the plasma membrane (*18*). Cell polarization at the edge of a wounded monolayer also depends on Cdc42 activity, and polarized cells demonstrate Cdc42 localization at their leading edges and on vesicles that appear to translocate from the tips of the cells toward the nucleus (*19*, *20*).

The timing of Cdc42 activation can be detected using a biochemical assay that allows selective immunoprecipitation of GTP-bound Cdc42 using a fusion protein of glutathione *S*-transferase and the Cdc42 effector PAK (*20*, *21*). However, since this assay requires disruption of cells, it does not allow simultaneous observation of Cdc42 localization and activation. Further, sensitivity issues may prevent detection in cases where very little Cdc42 is activated. Some of these limitations are overcome by immunostaining fixed cells with the GTPase binding domain (GBD) of a specific Cdc42 effector, such as the Wiskott−Aldrich syndrome protein (WASP). Such reagents have been used to detect the localization of activated Cdc42 at the immunological synapse in T cells (*11*). A GFP-GBD fusion protein has also been expressed in living cells to study the dynamic localization of active Cdc42 in response to cadherin signaling (*22*). However, this methodology is limited in the amount of quantitative information it can yield. Thus, to accurately study the temporal and spatial dynamics of Cdc42 in living cells, better tools need to be developed.

Recent studies have begun to address the spatial and temporal dynamics of GTPases using fluorescence resonance energy transfer (FRET) experiments. Kraynov et al. have developed a FRET-based method for measuring the activity of ectopically expressed Rac in microinjected cells (*23*). This method has also been used in fixed cells to study the spatial and temporal control of Rac activity in response to integrin signaling and changes in cell tension (*24*, *25*). Recently, Mochizuki et al. have reported the development of FRET-based sensors in which a Ras-Raf fusion protein is flanked by cyan fluorescent protein (CFP) and yellow fluorescent protein (YFP) (*26*). When the Ras moiety of this construct is loaded with GTP, intramolecular association with the Raf element leads to detectable changes in CFP-YFP FRET. This design is particularly advantageous because FRET occurs intramolecularly, which eliminates difficulties of fluorophore balance inherent in two-component FRET systems (*27*). In addition, the Ras sensor is genetically encoded, which facilitates use in a wide variety of systems.

Here we report the design and biochemical characterization of three novel classes of genetically encoded Cdc42 and Cdc42 GEF biosensors that utilize intramolecular FRET between CFP and YFP to monitor the activation and deactivation of the GTPase. The two classes of Cdc42 sensors are based on fluorophore-tagged fragments of WASP, which bind specifically to the active GTPase. In the GEF sensor, this basic fluorescent element is fused directly to Cdc42, enabling detection of GEF activity. Affinity measurements of the Cdc42 sensors reveal that the two fluorescent proteins only minimally interfere with the affinity of WASP for Cdc42. For the Cdc42 GEF sensors, the GEF-catalyzed GTP loading rate is nearly identical to that of wild-type Cdc42, but GAP-catalyzed hydrolysis is significantly slower than for the isolated GTPase. The Cdc42 sensors yield up to 3.2-fold changes in CFP-YFP emission ratios upon binding the activated GTPase. The GEF sensors give up to 1.7-fold FRET ratio changes upon GTP loading. In vivo, the Cdc42 sensors detect activity in cells expressing either a constitutively active mutant of Cdc42 or wild-type Cdc42 and GEF proteins. Similarly, the GEF sensors respond to overexpression of Cdc42 exchange factors. Thus, the sensors reported here represent a novel and promising class of genetically encoded probes for elucidating the processes involved in cellular signal transduction.

EXPERIMENTAL PROCEDURES

Plasmid Construction, Protein Expression, and Purification. To facilitate cloning of the sensor constructs, we engineered a modified pet11a bacterial expression vector (Novagen) containing the enhanced CFP (ECFP) and en-

[1] Abbreviations: CFP, cyan fluorescent protein; cps, counts per second; CRIB motif, Cdc42/Rac interactive binding motif; DH, Dbl homology; ECFP, enhanced cyan fluorescent protein; EYFP, enhanced yellow fluorescent protein; FcγR, Fc γ receptor; FRET, fluorescence resonance energy transfer; GAP, GTPase activating protein; GBD, GTPase binding domain; GDI, guanine nucleotide dissociation inhibitor; GEF, guanine nucelotide exchange factor; GFP, green fluorescent protein; GMPPNP, guanosine 5′-(β,γ-imidotriphosphate); K_d, dissociation constant; PAK, p21 activated kinase; PH, Pleckstrin homology; PBS, phosphate-buffered saline; WASP, Wiskott−Aldrich syndrome protein; YFP, yellow fluorescent protein.

hanced YFP (EYFP) genes (Clonetech) separated by a 5′ *Nco* site and a 3′ *Xho* site. To improve pH stability, the Q69K mutation was introduced into the EYFP gene using the QuikChange site-directed mutagenesis kit (Stratagene) (*28*). The ECFP-EYFP vector can be used to insert any gene containing a 5′ *Nco*I site and a 3′ *Xho*I site.

For all of the Cdc42 sensors, different WASP sequences (Table 1) were cloned from human cDNA. The WASP GBD-VCA sensors, containing GGS-GGS linker sequences, were cloned from constructs reported previously (*29*, *30*). Each sensor protein was expressed in *Escherichia coli* and purified by anion-exchange and hydrophobic exchange chromatography.

The GEF sensors were constructed by modifying the vector containing the N-WASP GBD-VCA sensor. Cdc42 residues 1−179, lacking the C-terminal prenylation motif, were inserted immediately N-terminal to the CFP moiety. For ease of purification, the GEF sensors were cloned into the pet15b vector (Novagen), which contains an N-terminal polyhistidine tag. Affinity purification on a Ni-NTA resin (Qiagen) was followed by anion-exchange chromatography.

For mammalian expression, a modified pCMV-Script vector (Stratagene) was used. An internal *Nde*I site was removed, and a new polylinker site with *Nde*I and *Bam*HI cloning sites was inserted into this vector. The resulting vector was named pASTO. A version of pASTO encoding a C-terminal HA tag, named pASTO-HA, was also created. Each sensor protein was then transferred into the pASTO vector using *Nde*I and *Bam*HI restriction sites.

Cdc42 was prepared and loaded with nucleotide as described previously (*31*).

A bacterial expression plasmid encoding the tandem Dbl and Pleckstrin homology (DH-PH) domains of DBS (residues 623−967) fused to a C-terminal polyhistidine tag was a gift from Dr. Sharon Campbell (University of North Carolina, Chapel Hill, NC) (*32*). Bacterially expressed DBS was purified as previously described (*32*).

A mammalian expression plasmid encoding SopE, a Cdc42/Rac GEF from *Salmonella typhimurium*, was a gift from Dr. Jorge Galan (Yale University, New Haven, CT) (*33*). Appropriate primers were used to transfer the SopE gene into pASTO-HA. Either the original plasmid or the pASTO-HA plasmid was used in the transfection assays.

The gene for FGD1, a mammalian Cdc42 GEF (residues 330−710), encoded in the pFlag mammalian expression vector was a gift from Dr. Yi Zheng (Cincinnati Children's Hospital Medical Center, Cincinnati, OH) (*34*).

The gene for YopE, a GAP from *Yersinia pestis*, was a gift from Dr. Kim Orth (UT Southwestern Medical Center, Dallas, TX). YopE (residues 51−219) was cloned into the pASTO-HA vector for mammalian expression and into a pet15b vector for bacterial expression.

Mammalian expression plasmids for Myc-tagged Cdc42V12 and RacV12, as well as plasmids for HA-tagged Cdc42N17 and RacN17, were kindly provided by Dr. J. Victor Garcia (UT Southwestern Medical Center, Dallas, TX).

Fluorescence Spectroscopy. All in vitro fluorescence measurements were carried out on a Fluorolog-3 spectrofluorometer (JY Horiba, Edison, NJ). All biochemical assays were performed at 25 °C in buffer containing 20 mM HEPES, pH 7.5, 150 mM KCl, 2 mM $MgCl_2$, and 2 mM DTT unless noted otherwise.

(A) Cdc42 Sensors. The ratio of 526 nm emission (maximum for YFP) to 476 nm emission (maximum for CFP) with 433 nm excitation (maximum for CFP) was recorded for each Cdc42 sensor in the presence or absence of saturating amounts of Cdc42 loaded with GMPPNP or GDP.

For affinity measurements, sensors were titrated with increasing amounts of Cdc42-GMPPNP. Data were fit to the following quadratic equation describing a single-site binding isotherm using GraphPad Prism version 3.0 software:

$$Y = (F_{max} - F_{init})\{(K_d + [\text{Cdc42}] + [\text{sensor}] - \{(K_d + [\text{Cdc42}] + [\text{sensor}])^2 - 4[\text{Cdc42}][\text{sensor}]\}^{0.5}/2[\text{sensor}]\} + F_{init}$$

where Y = measured fluorescence intensity, F_{max} = fluorescence intensity in the presence of saturating amounts of Cdc42, F_{init} = fluorescence intensity in the absence of Cdc42, [sensor] = total sensor concentration, [Cdc42] = total Cdc42 concentration, and K_d = dissociation constant for sensor−Cdc42 interaction.

Corrections for photobleaching and buffer volume were applied prior to fitting. Maximum changes in CFP-YFP emission ratio were determined with sensor concentration at K_d and Cdc42 concentration 10-fold above.

(B) GEF Sensors. The ratio of 526 nm emission (YFP) to 476 nm emission (CFP) with 433 nm excitation (CFP) was recorded for each GEF sensor either alone or after incubation with DBS and GMPPNP for 30 min, after which time nucleotide loading is complete. Experiments were performed in buffer containing 20 mM phosphate, pH 7.4, 2 mM $MgCl_2$, and 150 mM NaCl.

Nucleotide loading assays of wild-type Cdc42 were performed by incubating 100 nM GTPase with 400 nM DBS, 2 μM GMPPNP, and 100 nM N-GBD-VCA sensor. The decrease in YFP emission at 526 nm with CFP excitation at 433 nm was followed over the course of the experiment as a reporter of the loading reaction. Nucleotide loading assays of the GEF sensors were performed by incubating 100 nM sensor, 400 nM DBS, and 2 μM GMPPNP. The loss of YFP emission from the GEF sensor itself was used to monitor loading.

Nucleotide hydrolysis assays were performed by first incubating 1 μM sensor protein with 2 mM EDTA and 20 μM GTP in order to allow nucleotide loading. After loading was complete, nucleotide hydrolysis was initiated by addition of 4 mM $MgCl_2$ and YopE. Both loading and hydrolysis assays were performed in the absence of DTT.

Cell Culture and Microscopy. NIH 3T3 cells were maintained in Dulbecco's modified Eagle medium (DMEM) containing 10% fetal bovine serum (Invitrogen). Transfections were performed using Lipofectamine Plus (Invitrogen) in serum-free DMEM. Transfected cells were maintained in glass-bottom 35 mm dishes (MatTek Corp., Ashland, MA). Cells were imaged at 25 °C 30−36 h after transfection in Hank's balanced salt solution (Invitrogen) using a Zeiss Axiovert 200M microscope equipped with a 75 W xenon lamp.

FRET images were generated using a 63× oil immersion objective, 4 × 4 binning, and the 86002v2 fluorescence filter and dichroic mirror set (Chroma Technology Corp.). For each

cell, three images, CFP, YFP, and FRET, were captured. CFP and YFP images were acquired using CFP excitation and emission filters and YFP excitation and emission filters, respectively. FRET images were acquired by using the CFP excitation filter and the YFP emission filter. Plates of transfected cells were scanned using a 1% neutral density (ND) filter to prevent photobleaching, while images were acquired with a 10% ND filter. Typically, exposure times of 100−500 ms were used to capture the fluorescence images. Background subtraction was based on regions of each plate lacking cells. Quantitative measurements were typically based on cells exhibiting fluorescent intensities at least 25% above background. Images were collected using a Sensicam CCD camera (PCO Computer Optics GmbH, Germany) and analyzed with Slidebook version 3.0.10.3 software (Intelligent Imaging Innovations, Denver, CO). Each imaging experiment was repeated independently at least three times, and a minimum of 10 cells were analyzed per experiment.

Western Blot Analysis. To analyze sensor expression in vivo, NIH 3T3 cells were plated in six-well dishes and transfected as described above. Thirty-six hours after transfection, cells were washed with cold phosphate-buffered saline (PBS) and resuspended in lysis buffer (20 mM Tris, pH 7.5, 150 mM NaCl, 0.5% NP-40, 50 mM NaF, 1 mM $NaVO_3$, 0.5 mM PMSF, 5 μg/mL leupeptin, and 0.2 mM EGTA). After the cells were lysed on ice for 10 min, the samples were centrifuged, and the resulting supernatants were collected. Samples were normalized for protein content using the Coomassie Plus protein assay (Pierce) and run on an SDS−PAGE gel. Western blotting to detect sensor expression was performed with primary mouse αGFP antibodies (Santa Cruz) and alkaline phosphatase conjugated secondary antibodies (Promega). Proteins were visualized using colorimetric methods (Promega).

RESULTS

Design Strategy. WASP is a specific Cdc42 effector, unlike proteins such as PAK that can bind both Cdc42 and Rac (*8*). The C-terminal region of WASP, termed the VCA, binds to the ARP 2/3 complex and activates actin polymerization (Figure 1A) (*35*, *36*). The N-terminal GBD is comprised of the CRIB motif, as well as other sequence elements that are necessary for high-affinity interactions with Cdc42 (Figure 1A) (*37*, *38*). Free WASP exists in an autoinhibited conformation in which the GBD interacts intramolecularly with the VCA (*29*, *39*, *40*). Release of VCA, by disruption of the autoinhibited structure upon binding of active Cdc42 to the GBD, appears to be a key biochemical event in the activation of WASP (*29*−*31*).

The solution structure of the GBD bound to Cdc42, determined previously in our laboratory, reveals that the CRIB motif forms an intermolecular β-sheet with the β2 strand of Cdc42 (Figure 1B). The structure of the GBD then terminates in a β-hairpin and α-helix unit, which packs against the switch I and II regions of the GTPase. The autoinhibited GBD-VCA structure shows that the GBD exists as an N-terminal β-hairpin and α-helix packed against four α-helices, one of which is contributed by VCA (Figure 1C) (*29*). Thus, the N-terminal half of the GBD binds to Cdc42 while the C-terminal half binds to VCA. However, the GBD cannot simultaneously bind both Cdc42 and VCA because

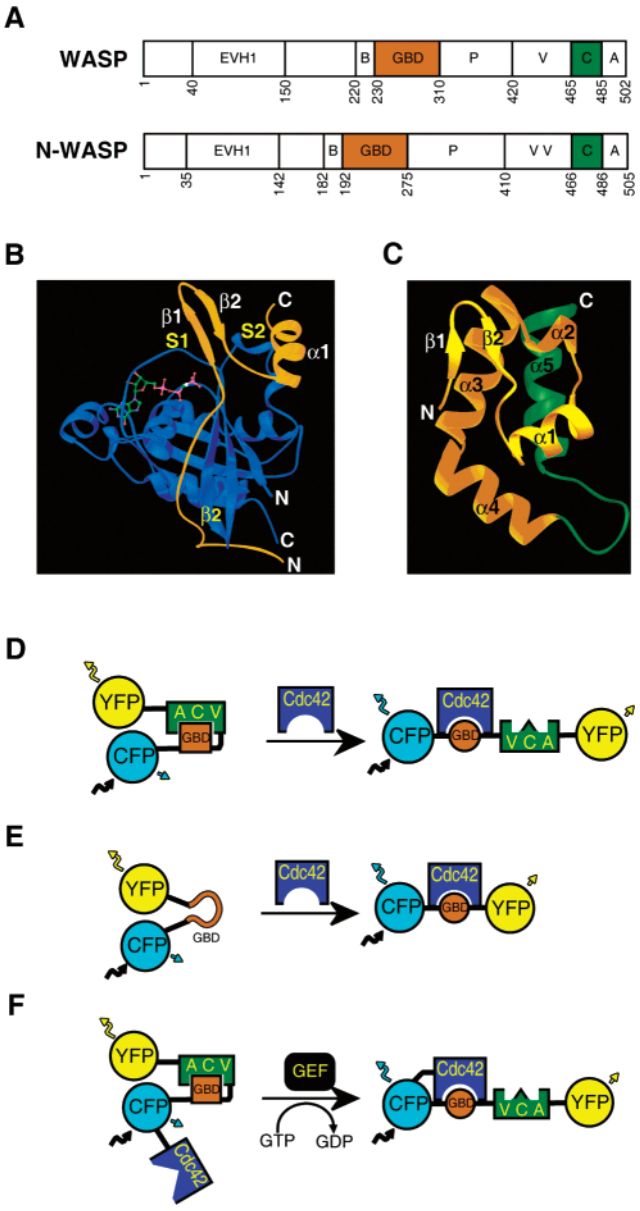

FIGURE 1: Conceptual design of FRET-based sensors of Cdc42 signaling. (A) Domain structure of WASP and N-WASP. The domains of WASP and N-WASP include an enabled/VASP homology 1 domain (EVH1), basic region (B), GTPase binding domain (GBD), polyproline region (P), verprolin homology region (V), central hydrophobic region (C), and acidic region (A). Note that N-WASP contains two tandem V regions. (B) Structure of Cdc42-GMPPNP bound to the GBD (residues 230−288) of WASP (*31*, *55*). The GBD is in orange, Cdc42 is in blue, and nucleotide is shown as a stick figure. The N and C termini are labeled. Secondary structure elements are labeled in white for the GBD and yellow for Cdc42. S1 = switch I, and S2 = switch II. (C) Structure of the autoinhibited WASP domain (residues 242−310-GGSGGS-460−492) (*29*, *55*). The GBD is in orange, and the C region of VCA is in green. The N and C termini are labeled. (D) Schematic representation of GBD-VCA FRET-based sensors of Cdc42 activation. (E) Schematic representation of GBD-only FRET-based sensors of Cdc42 activation. (F) Schematic representation of FRET-based sensors of Cdc42 GEF activation.

the central β-hairpin and α-helix unit is essential to the formation of either complex. The structural studies demonstrate that the autoinhibited fold is incompatible with the Cdc42-bound structure of the GBD and that binding of Cdc42 must result in a marked conformational change of the autoinhibited complex.

Table 1: Properties of the Cdc42 Sensors[a]

sensors	description	K_d for Cdc42 (nM)	unbound FRET	bound FRET	in vitro ratio	transfected alone	transfected with Cdc42V12	in vivo ratio
GBD only								
B-CRIB	hWASP 225−251	133 ± 8	3.70	2.46	1.50	2.52 ± 0.16	2.09 ± 0.38	1.21
B-GBD1	hWASP 225−288	15 ± 3	2.45	1.66	1.47	1.81 ± 0.11	1.70 ± 0.13	1.06
GBD1	hWASP 230−288	19 ± 2	2.35	1.25	1.87	1.94 ± 0.11	1.37 ± 0.14	1.42
GBD2	hWASP 230−310	92 ± 6	2.50	1.50	1.66	1.93 ± 0.23	1.32 ± 0.08	1.46
GBD-VCA								
B-GBD-C	hWASP 225−310-GGSGGS-461−492	700 ± 38	2.28	1.18	1.94	1.52 ± 0.19	1.26 ± 0.08	1.21
B-GBD-VCA	hWASP 225−310-GGSGGS-420−502	1300 ± 98	2.63	1.03	2.56	1.84 ± 0.32	1.03 ± 0.12	1.79
N-GBD-VCA	hN-WASP 192−275-GGSGGS-393−505	178 ± 3	2.23	0.69	3.24	1.66 ± 0.06	0.96 ± 0.03	1.73
N-GBD-DD-VCA	hN-WASP 192−275-GGSGGS-393−505 H211D,H214D	>250000	2.14	2.04	1.05	1.76 ± 0.05	1.41 ± 0.07	1.25

[a] The residues of human WASP (hWASP) or human N-WASP (hN-WASP) that comprise each sensor are listed. Each of the GBD-VCA sensors contains a (Gly-Gly-Ser)$_2$ linker between the GBD and VCA regions. K_d values are based on the results of three independent titrations with Cdc42 loaded with GMPPNP. Errors were calculated during curve fitting. For the mutant N-GBD-DD-VCA sensor, in vitro FRET values have been determined with the same concentration of Cdc42 as for the wild-type sensor (10 μM; see text).

On the basis of the structural data, we hypothesized that appropriate fluorophores fused to the termini of the GBD-VCA construct should display measurable changes in intramolecular FRET upon Cdc42 binding (Figure 1D). In addition, since the isolated GBD is unstructured in solution, FRET changes in response to Cdc42 should occur in a fluorophore-tagged GBD-only construct as well (Figure 1E) (*29*, *38*). We also developed a third class of sensors that would respond directly to Cdc42 GEFs. In these constructs, Cdc42 is fused directly to the fluorophore-flanked GBD-VCA proteins. This sensor protein should be a substrate for GEFs, and the covalent tethering of the GTPase to its effector should favor intramolecular binding of the GBD and activated Cdc42 (Figure 1F).

Since our aim was to develop sensors for Cdc42 signaling that could be used in living systems, we chose the genetically encoded fluorophores CFP and YFP, whose fluorescence emission and absorption spectra are well-matched for FRET (*41*). Sensors were developed using sequences from both WASP and its homologue N-WASP. To optimize FRET changes upon activation, we created many constructs containing different GBD and VCA structural elements and surrounding residues (Table 1).

In Vitro Characterization of Sensors. (A) Cdc42 Sensors. Initially, four different GBD-only sensor constructs were created, each containing different portions of the GBD and surrounding residues. All of the purified sensors exhibit a high FRET value (yellow to cyan emission ratio) upon excitation of CFP when alone in solution (Table 1, unbound FRET) with values ranging from 2.35 to 3.70. Upon addition of Cdc42 loaded with GMPPNP, a GTP analogue, all of the sensors show significantly decreased FRET values (Table 1, bound FRET) ranging from 1.25 to 2.46. The ratio between the initial, unbound FRET and the final, bound FRET ranges from 1.47 for the B-GBD1 sensor to 1.87 for the GBD1 sensor (Table 1, in vitro ratio). These results are consistent with our hypothesis that binding of activated Cdc42 to an unstructured GBD-only construct can induce a significant conformational ordering, which is detectable by FRET. Moreover, the large magnitude of FRET change for the GBD1 sensor suggests that this construct may be useful for in vivo applications.

Next, we focused on development of the GBD-VCA sensors. Like the GBD-only sensors, each of the purified GBD-VCA sensors exhibits a high FRET value, ranging from 2.23 to 2.64, when alone in solution. In all cases, addition of Cdc42-GMPPNP causes a significant decrease in FRET, with final values ranging from 0.69 to 1.18 (Table 1). The B-GBD-C sensor, which contains the minimal portion of the VCA involved in GBD binding, yields a FRET ratio change of 1.9-fold, which is similar to the result for the GBD1 sensor. However, B-GBD-VCA, which contains the full VCA sequence, gives a much higher FRET change of 2.6-fold. A GBD-VCA sensor derived from N-WASP, called N-GBD-VCA, yields the highest FRET change, 3.2-fold, of any sensor tested (Figure 2A).

The observation that the unbound FRET is always greater than the bound FRET supports the idea that addition of Cdc42 causes separation of the two fluorophores. For each of the GBD-VCA sensors, the bound FRET value decreases as the length of the linker between GBD and C increases. Thus, B-GBD-VCA has a lower bound FRET than B-GBD-C (1.03 vs 1.18, respectively), while N-GBD-VCA, which has an additional 27 amino acids in the linker as compared to B-GBD-VCA, has the lowest bound FRET value of 0.69 (Figure 2, Table 1). The correlation between bound FRET and linker length for the GBD-VCA sensors supports our hypothesis that binding of Cdc42 substantially disrupts the structure of the autoinhibited WASP domain.

Control experiments were performed to ensure that binding of Cdc42-GMPPNP to the sensor is responsible for the observed FRET changes. Cdc42-GDP did not induce FRET changes in either the GBD2 sensor (data not shown) or the N-GBD-VCA sensor (Figure 2A). Mutation of two conserved histidine residues in the CRIB motif (residues 211 and 214 in N-WASP) to aspartate has been shown to significantly decrease affinity for Cdc42 (*42*). When these mutations are introduced into the N-GBD-VCA sensor, the mutant protein, N-GBD-DD-VCA, has an initial FRET value of 2.14. Addition of Cdc42-GMPPNP at levels sufficient to saturate the wild-type sensor decreases the FRET slightly, to a value of 2.04 (Figure 2B). The GBD2 sensor with analogous mutations also has a much weaker response to Cdc42-GMPPNP (data not shown). The slight decreases in FRET for these two mutant sensors are attributed to the residual affinity of the mutants for Cdc42, as discussed below. These results show that both the GBD-only and GBD-VCA sensor proteins are specific for the activated state of Cdc42 and

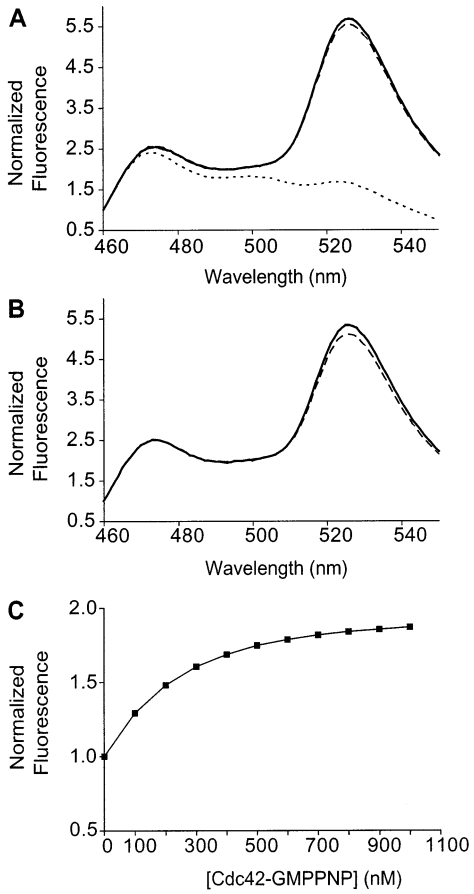

FIGURE 2: Biochemical characterization of GBD-VCA sensors. Fluorescence emission spectra (excitation wavelength, $\lambda_{ex} = 433$ nm) of (A) 0.2 μM N-GBD-VCA sensor free (—) and in the presence of 10 μM Cdc42-GMPPNP (---) or 10 μM Cdc42-GDP (— —) and (B) 0.2 μM N-GBD-DD-VCA sensor free (—) and in the presence of 10 μM Cdc42-GMPPNP (---). Spectra are normalized to the emission at 460 nm. (C) Titration of 0.1 μM N-GBD-VCA sensor with Cdc42-GMPPNP. Changes in CFP emission ($\lambda_{em} = 476$ nm) are shown. The spectrum is normalized to the fluorescence emission in the absence of Cdc42. The line calculated by fitting the data to a single-site binding model is shown. Standard deviations of each value, determined from three independent titrations, are smaller than the data symbols.

that binding of the GTPase to the sensor protein is necessary for changes in FRET.

We used the GTPase-induced fluorescence changes to measure the binding affinity of each of the sensors for Cdc42-GMPPNP. Changes in either CFP fluorescence or YFP fluorescence could be modeled to an equation describing a 1:1 stoichiometric binding event to determine a dissociation constant (K_d) for the Cdc42—sensor interaction. The CFP-based binding curve for the N-GBD-VCA sensor yields a K_d of 178 nM (Figure 2C). As a control, sedimentation equilibrium analytical ultracentrifugation was used to demonstrate that the N-GBD-VCA sensor is indeed monomeric under the conditions of our in vitro assay (data not shown). The affinity measurements for all of the other GBD and GBD-VCA sensors are listed in Table 1. In all instances, the GBD-only sensors have appreciably higher affinity for Cdc42-GMPPNP than the GBD-VCA sensors. These results are consistent with a model in which Cdc42 binding causes significant conformational rearrangement of the autoinhibited GBD-VCA structure and where the energy used to drive this change is drawn from energy inherent in the GBD-GTPase contacts (*29*, *30*).

In parallel experiments, the affinities of the N-GBD-VCA and GBD1 sensors for Rac1-GMPPNP were determined to be 19.8 ± 0.8 μM and 22.2 ± 0.6 μM, respectively (data not shown). These results establish that our WASP-based biosensors have 100—1000-fold specificity for activated Cdc42 over activated Rac.

Titration of the N-GBD-DD-VCA mutant sensor yielded measurable FRET changes at relatively high concentrations of Cdc42-GMPPNP. Our results indicate that the H211D/H214D mutations reduce the affinity of Cdc42 for the GBD from 178 nM to at least 250 μM, a difference of more than 1000-fold (Table 1). Thus, although these mutations have been reported to qualitatively abrogate GTPase binding, some residual affinity remains and binding will occur at high protein concentrations (*42*).

Our FRET-based affinity measurements for WASP—Cdc42 interactions are consistent with the values measured by isothermal titration calorimetry, and both methods yield affinities that are approximately 7-fold higher than the widely used strategies employing fluorescently labeled GMPPNP (*38*, *43*).

(B) GEF Sensors. The GEF sensors were constructed by fusing wild-type Cdc42 to the N-terminus of the N-GBD-VCA sensor. We prepared several sensors with variable length linkers containing $(Gly\text{-}Gly\text{-}Ser)_n$, or $(GGS)_n$, repeats between Cdc42 and the rest of the molecule. The sensors were assayed for their ability to detect GMPPNP loading upon incubation with the DH-PH unit of DBS, a GEF that is active toward Cdc42 and Rac. None of these first-generation GEF sensors display significant FRET changes upon GMPPNP loading (Figure 3A and data not shown). All of the GEF sensors share the common feature that their GDP FRET values are much lower than those of any of the GBD-only or GBD-VCA sensors described above. For example, the GEF sensor with a linker comprising four tandem GGS repeats (referred to as wild type in Table 2), which was used for subsequent optimization of the GEF sensors, gives a GDP FRET value of only 1.06 while the isolated N-GBD-VCA sensor has a FRET value of 2.14 (Figure 3A, Table 2). The GTP FRET value for the wild-type GEF sensor is 0.91 compared to 0.71 for the N-GBD-VCA sensor. Thus, the original GEF sensors have poor FRET changes because of both decreased GDP FRET values and increased GTP FRET values as compared to the Cdc42 sensor. However, the main factor contributing to weak FRET changes is the very low GDP ratio.

We hypothesized that the lower GDP FRET values for the GEF sensors could be caused by intramolecular binding of Cdc42 to the GBD even in the GDP-loaded state. We sought to test this hypothesis by introducing mutations within the GBD portion of the sensor that would differentially affect intramolecular contacts in the GDP- and GTP-bound states.

Structural and biochemical data suggest that N-terminal portions of the CRIB motif make energetically important contacts to regions of Cdc42 that are only minimally affected by the nucleotide switch (*31*, *37*, *40*, *44*, *45*). Using the structural data for the WASP GBD as a model for N-WASP, we focused our mutagenesis efforts on four residues in this region of the N-WASP GBD, L198, I203, P206, and F209. The latter three residues are fully conserved within the CRIB

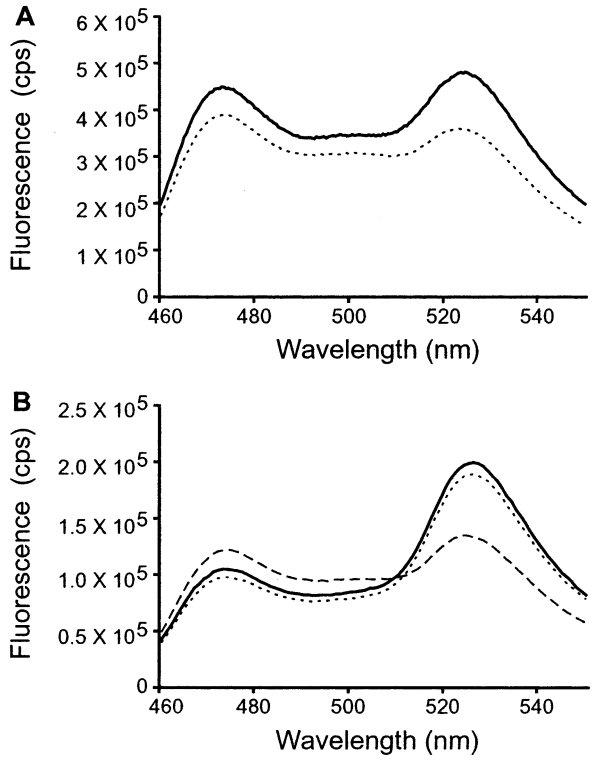

FIGURE 3: Fluorescence emission spectra of the Cdc42 GEF sensors. Fluorescence emission spectra (λ_{ex} = 433 nm) of (A) the wild-type GEF sensor in the GDP state (—) or after GMPPNP loading by DBS (---) or (B) the L198K GEF sensor in the GDP state (—) or after GMPPNP (— —) or GDP (---) loading by DBS. For the DBS experiments, the sensor was incubated with DBS and nucleotide, and the system was allowed to reach equilibrium.

Table 2: Properties of the Cdc42 GEF Sensors[a]

description	GDP FRET	GTP FRET	in vitro ratio
wild type	1.06	0.91	1.16
L198A	1.38	0.92	1.50
L198K	1.89	1.11	1.70
L198D	1.41	0.96	1.47
I203A	1.73	1.50	1.15
P206A	1.37	0.93	1.47
F209A	1.19	1.19	1.00
H211D/H214D	1.24	1.15	1.08

[a] The wild-type GEF sensor refers to the construct in which Cdc42 was fused to the N-GBD-VCA sensor. Each of the mutations indicated were introduced into the coding region of the wild-type sensor.

motif. Mutation of each of the four residues to alanine affects the FRET ratio as shown in Table 2. The I203A and F209A mutants both yield poor overall FRET changes of 1.15-fold and 1.00-fold, respectively, upon GMPPNP loading. However, both the L198A and P206A mutants are greatly improved sensors of GEF activity as they have higher GDP ratios while maintaining low GTP ratios, yielding overall FRET changes of 1.50 and 1.47, respectively.

Further support of our intramolecular binding hypothesis comes from data for a GEF sensor with the H211D/H214D mutations, which inactivate the Cdc42 sensors described above. These histidines contact switch I of Cdc42 in a manner only possible in the GTP-bound state (*31*). Consistent with this role, the double mutation affects the GTP FRET value more significantly than the GDP FRET value, such that the overall FRET change of 1.08 is significantly reduced compared to the wild-type sensor. Thus, as expected, the H211D/H214D mutant is a poorer sensor of GTP loading than the wild-type molecule.

Next, we attempted to optimize the L198A GEF sensor further by introducing more severe mutations at residue 198 (Table 2). Of these, the L198K mutant proves to be the best GEF sensor in vitro, yielding a GDP FRET value of 1.89 and a GTP FRET value of 1.11 (Figure 3B). As a control, addition of DBS and GDP had no effect on the FRET value (Figure 3B). With an overall FRET change of 1.70, the L198K mutant is an extensively optimized molecule that functions as an effective GEF sensor.

To determine whether the L198K GEF sensor is likely to report accurately on the timing of Cdc42 activation and deactivation in vivo, we measured its rates of nucleotide loading and hydrolysis. DBS-catalyzed rates of GMPPNP loading were investigated for the L198K GEF sensor and wild-type Cdc42. The intrinsic FRET of the L198K GEF sensor was used to measure its loading rate, while FRET changes in the N-GBD-VCA sensor were used to quantitate loading of wild-type Cdc42. Under identical conditions, the L198K GEF sensor and wild-type Cdc42 are loaded with GMPPNP at essentially identical rates of 0.016 s^{-1} and 0.014 s^{-1}, respectively (Figure 4A). These results suggest that the GEF sensors will accurately report the activation kinetics of Cdc42 in vivo.

To compare the deactivation kinetics of the L198K GEF sensor and wild-type Cdc42, we measured the rate of GTP hydrolysis in the presence of YopE, a GAP protein from *Y. pestis* (Figure 4B) (*46*). GTP hydrolysis by wild-type Cdc42 was monitored by tryptophan fluorescence, which is sensitive to the nucleotide state of the protein (*47*). Nucleotide hydrolysis in the L198K GEF sensor was monitored by FRET and tryptophan fluorescence, which provided identical results (Figure 4B and data not shown). If the sensor was first loaded with GMPPNP, which cannot be hydrolyzed readily, addition of YopE had no effect on FRET, confirming that recovery of FRET in experiments with GTP is due to hydrolysis of the nucleotide in the Cdc42 portion of the sensor (data not shown).

For both Cdc42 and sensor, the nucleotide hydrolysis rate is linearly dependent on the concentration of YopE (Figure 4B,C). However, for all YopE concentrations that could be directly compared, the initial hydrolysis rate is 16-fold slower for the L198K GEF sensor than for wild-type Cdc42 (Figure 4C). In addition, the time to reach half-maximal saturation of FRET recovery is greater for the L198K GEF sensor than for wild-type Cdc42 at each concentration of YopE tested (Figure 4D). The magnitude of the difference between $t_{1/2}$ values depends on the YopE concentration. Therefore, the ability of the sensor to accurately mirror the kinetics of Cdc42 deactivation in vivo will depend on the local cellular concentration of active GAP protein.

Structural studies of Cdc42−GAP complexes have demonstrated that GAP and effectors interact with similar regions of the GTPase (*31*, *40*, *44*, *48*, *49*). Although the mechanism by which GAPs access GTPase−effector complexes is not well understood, it is reasonable that the high local concentration of N-WASP in the tethered GEF sensor could hamper this process, thereby reducing the sensitivity of the sensor to GAP. While this issue has not been addressed in other GEF and GTPase sensors, it is likely to be a general problem in this class of reagents (*23*−*26*). Taken together, these

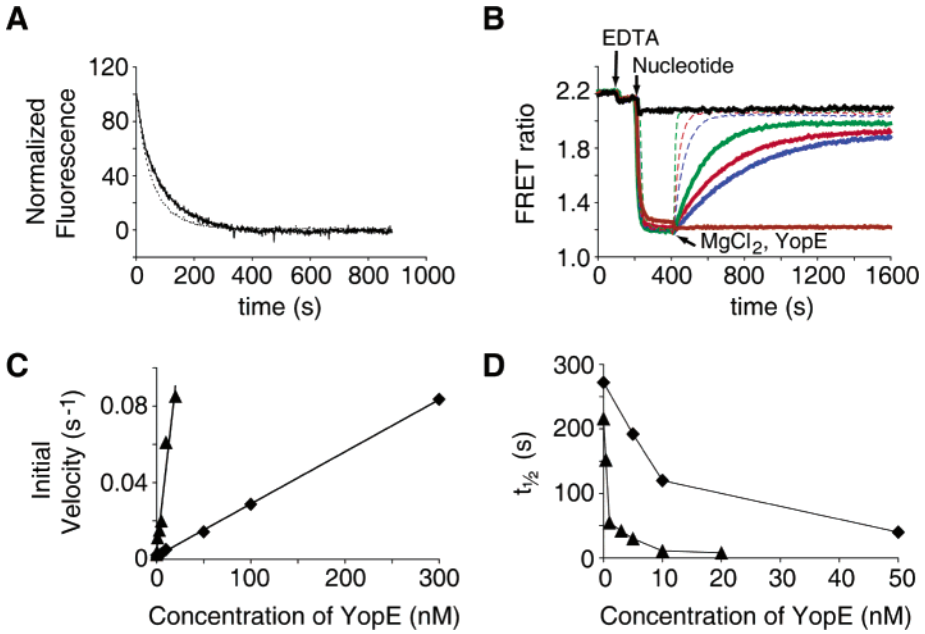

FIGURE 4: Biochemical characterization of the L198K GEF sensor. (A) Nucleotide loading assays with 100 nM L198K GEF sensor (---) and 100 nM wild-type Cdc42 (—). The loading of 2 μM GMPPNP by 400 nM DBS was monitored by FRET (CFP excitation, $\lambda_{ex} = 433$ nm, and YFP emission, $\lambda_{em} = 526$ nm) for both experiments. For GEF sensor loading, emission changes in the sensor itself were measured. For Cdc42, loading was performed in the presence of 100 nM N-GBD-VCA sensor, which yielded FRET emission changes as the reaction progressed. For each experiment, the final fluorescence was set as baseline, and all of the data were normalized to the initial fluorescence value. The initial velocities are 0.016 s^{-1} for the L198K GEF sensor and 0.014 s^{-1} for wild-type Cdc42. (B) GAP-stimulated nucleotide hydrolysis assays with 1 μM L198K GEF sensor. Hydrolysis was monitored by FRET recovery. Components of the reaction were added at the time points indicated by the arrows. The decrease in FRET value upon addition of 2 mM EDTA and 20 μM GTP corresponds to loading of GTP onto the sensor. In the absence of $MgCl_2$, the Cdc42 moiety of the sensor is unable to hydrolyze bound nucleotide. Addition of 4 mM $MgCl_2$, allows the GTPase reaction to proceed. The concentration of YopE in each experiment is as follows: 0 (blue solid line), 5 (red solid line), 10 (green solid line), 50 (blue dotted line), 100 (red dotted line), and 300 nM (green dotted line). Control experiments with GDP (black solid line) and GMPPNP (brown solid line) are also shown. (C) Initial velocity of GTP hydrolysis by the L198K GEF sensor (◆) obtained from (B) and 1 μM wild-type Cdc42 (▲) obtained from tryptophan fluorescence (data not shown) vs concentration of YopE. Slopes are 0.00027 s^{-1} nM^{-1} for the L198K GEF sensor and 0.0043 s^{-1} nM^{-1} for wild-type Cdc42. (D) Nucleotide half-life vs concentration of YopE for the L198K GEF sensor (◆) obtained from (B) and for wild-type Cdc42 (▲) obtained from tryptophan fluorescence experiments (data not shown).

results show that the GEF sensor will be able to reliably detect the timing of Cdc42 pathway activation. However, inactivation data will have to be carefully interpreted, and it may be difficult to accurately monitor processes that depend on rapid turnover of GTP.

Measurement of FRET in Living Cells Using Cdc42 Sensors. The ability of the Cdc42 sensors to measure GTPase activity in vivo was assessed using transiently transfected NIH 3T3 cells. Cells were transfected either with sensor alone or with sensor and Cdc42V12, a constitutively active mutant. FRET values were calculated by measuring the intensity of light emitted through CFP and YFP filters in response to sample excitation through a CFP filter. FRET values for an entire cell were measured by averaging the FRET at every point in the cell. The amount of sensor at each point was assumed to correlate with the intensity of YFP emission upon YFP excitation (*27*). Representative cell images color-coded for FRET and intensity-normalized for sensor amount are shown in Figure 5, and whole cell FRET values are shown in Figure 6. Cells transfected with N-GBD-VCA sensor alone have an average FRET value of 1.66, compared to an initial FRET value of 2.23 in vitro (Figures 5A and 6A, Table 1). The sensor appears to be uniformly distributed, and most of the transfected cells maintain the spindled morphology typical of NIH 3T3 cells. The average FRET value decreases to 0.96 in cells cotransfected with sensor and Cdc42V12 (Figures 5A and 6A). The cells also become less elongated, and sensor staining in the nucleus is observed to decrease. The overall FRET change for N-GBD-VCA is 1.7-fold in vivo, which compares favorably to analogous CFP/YFP-based sensors reported in the literature, but is 47% less than the 3.2-fold FRET change obtained in vitro (Table 1). Each of the Cdc42 sensors was tested in the in vivo assay, and in each case, cells transfected with sensor alone have a significantly higher FRET value than those cotransfected with sensor and Cdc42V12 (Table 1). The reduction in FRET change between the in vivo and in vitro experiments is greatest for N-GBD-VCA as the rest of the sensors show only 20−30% reductions. Despite the reduction of FRET change, each of the sensors does accurately report Cdc42 activity in vivo, and in general, the sensors with the largest FRET changes in vitro also show the largest changes in vivo. The best in vivo sensor is B-GBD-VCA, which shows a 1.8-fold change in FRET in cells expressing activated Cdc42.

Several control experiments were performed with N-GBD-VCA to ensure that the FRET changes observed in cells are due to specific interactions between the sensor and activated Cdc42. When cells were cotransfected with sensor and wild-type Cdc42 or Cdc42N17, a dominant inhibitory mutant which is believed to act by sequestering GEFs from wild-type GTPase, no significant reduction in FRET was observed (Figures 5A and 6A) (*50*). Further, no FRET changes were measured in cells cotransfected with sensor and RacV12 or

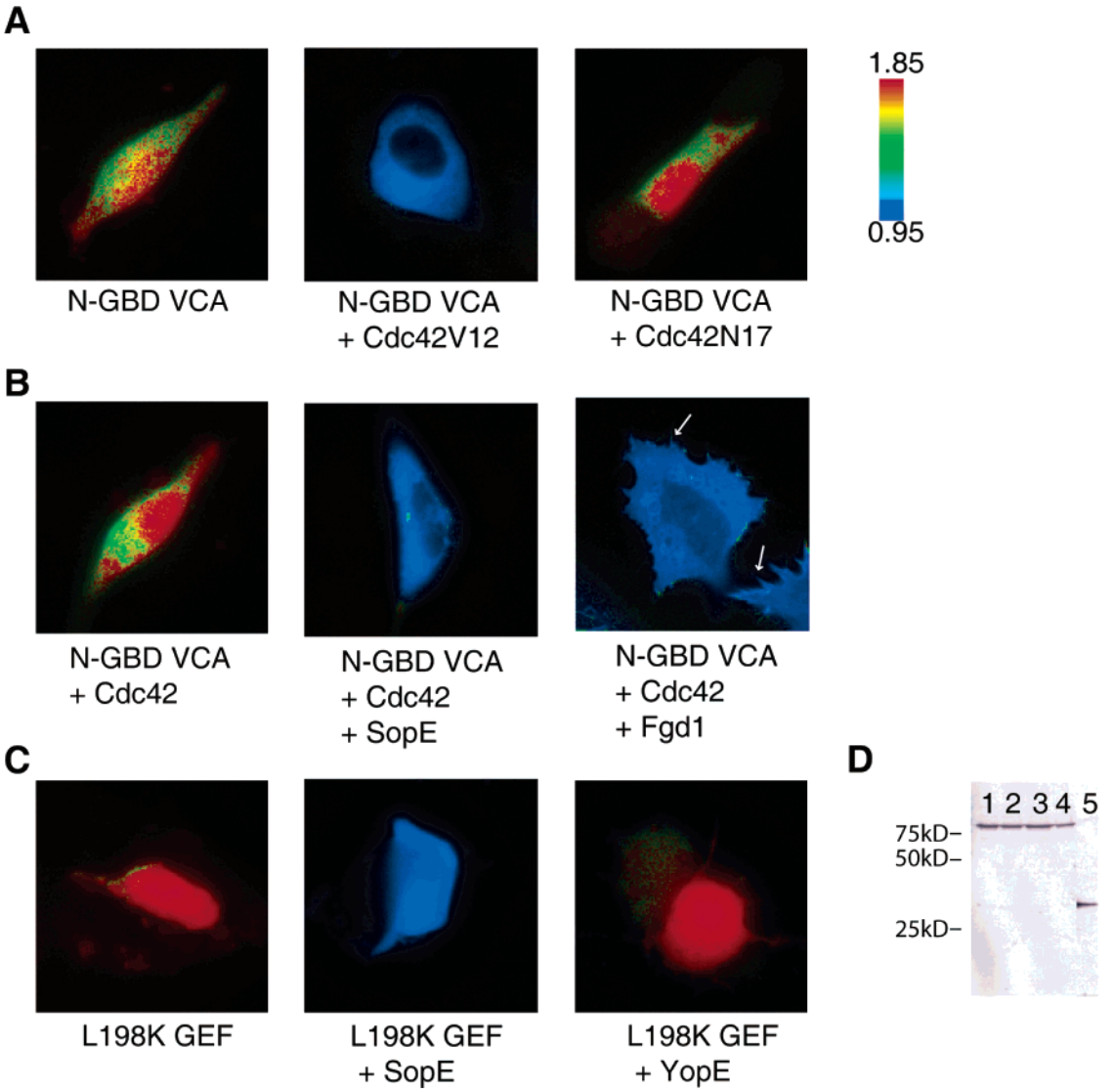

FIGURE 5: FRET images of transiently transfected NIH 3T3 cells. Cells were transfected with plasmids encoding the constructs indicated below each panel. Images have been color-coded to represent the sensor concentration and FRET value [(YFP channel emission intensity)/(CFP channel emission intensity) upon CFP excitation] distribution throughout the cell. Color hues correspond to the FRET value. The numerical FRET range described by the color hues is depicted in the spectral bar adjacent to the panel of images. The intensity of each pixel is determined by the YFP channel intensity, which correlates with total sensor amount, at that position. Arrows indicate the position of filopodia. Images are representative of the results obtained after analyzing at least 10 cells from a minimum of three independent experiments for each condition. Experiments were conducted with (A, B) the N-GBD-VCA sensor and (C) the L198K GEF sensor. (D) Western blots, stained with αGFP antibodies, demonstrating sensor expression in cells transfected with plasmids encoding (lane 1) N-GBD-VCA, (lane 2) N-GBD-VCA + Cdc42V12, (lane 3) N-GBD-DD-VCA, (lane 4) N-GBD-DD-VCA + Cdc42V12, and (lane 5) GFP.

RacN17 (Figure 6A), consistent with our in vitro results, indicating that the sensor is a specific monitor of Cdc42 activity in vivo. Finally, western blot analysis reveals that the observed changes in FRET are not due to sensor degradation, which could produce an artifactual decrease in FRET (Figure 5D).

In the presence of Cdc42V12, the N-GBD-DD-VCA mutant sensor did show a slight decrease in FRET value from 1.7 to 1.4, although the overall change is much less than for the wild-type sensor (Figure 6A). In the context of our transient transfection assay, we attribute this result to the residual affinity of the mutant sensor for active GTPase. This is reasonable given our measured K_d value of 250 μM for the interaction between mutant sensor and Cdc42 and previous reports that transiently expressed fluorescent proteins can reach cellular concentrations as high as 800 μM using standard transfection protocols (*28*).

We next examined whether the sensors could detect activation of wild-type Cdc42 upon stimulation with GEF by cotransfecting cells with sensor, Cdc42, and exchange factor. The FRET value decreases dramatically in these multiply transfected cells containing either SopE, a potent Cdc42 exchange factor from *S. typhimurium*, or the DH-PH module of Fgd1, a mammalian Cdc42 exchange factor (Figures 5B and 6B) (*33*, *34*). To test whether the sensors could detect activation of endogenous Cdc42, we cotransfected cells with only sensor and exchange factor. However, these conditions do not elicit detectable FRET changes in NIH 3T3 cells (Figure 6B). Therefore, with the technical conditions used for the present set of experiments, the sensors can detect activation of overexpressed wild-type Cdc42 but not endogenous protein.

Compared to cells cotransfected only with sensor and GEF, which have average FRET values of 1.76 and 1.69 for SopE

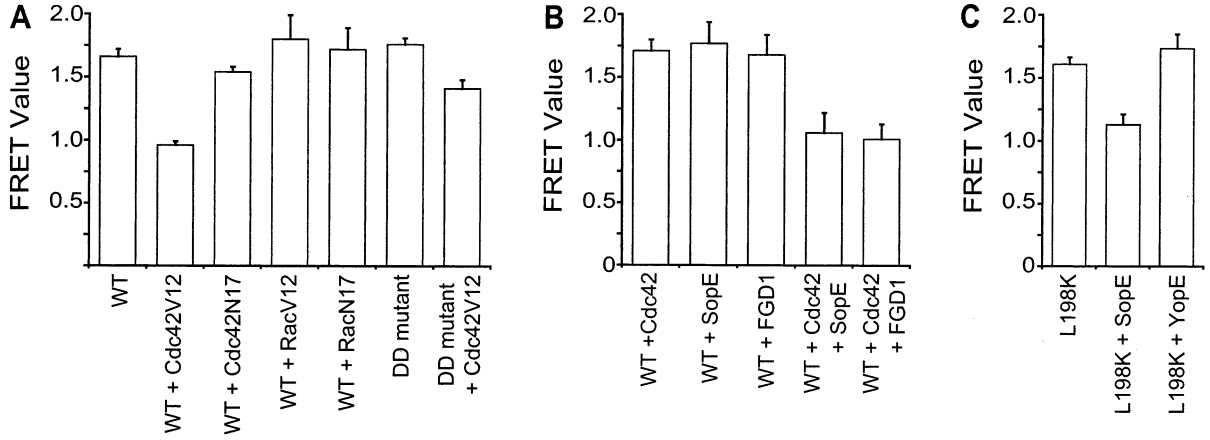

FIGURE 6: Quantitation of cellular FRET values. Each bar represents the average cellular FRET value [(YFP channel emission intensity)/(CFP channel emission intensity) upon CFP excitation] of 10 cells transfected with the indicated plasmids. Standard deviations are shown for a minimum of three indpendent transfections for each condition. (A) Experiments with the N-GBD-VCA sensor, labeled as WT, and N-GBD-DD-VCA sensor, labeled as DD mutant, and various Rho GTPase mutants. (B) Experiments with the N-GBD-VCA sensor, labeled as WT, and Cdc42 GEFs (SopE or FGD1). (C) Experiments with the L198K GEF sensor, labeled as L198K, and GEF (SopE) or GAP (YopE) proteins.

and FGD1, respectively, cells cotransfected with sensor, GEF, and wild-type Cdc42 yield FRET values of 1.06 and 1.01. Thus, similar to the results with overexpression of Cdc42V12, transfection of either SopE or FGD1 into Cdc42-supplemented cells causes a 1.7-fold reduction in FRET. Both SopE and FGD1 induced filopodia and membrane ruffling, presumably due to GTPase activity, in the Cdc42-supplemented cells. However, the effect of FGD1 is significantly greater in terms of number of filopodia per cell (Figure 5B). As a control, cells cotransfected with only sensor and Cdc42 do not display any significant morphological changes and have a high FRET value of 1.71, indicating that Cdc42 is not active on its own (Figures 5B and 6B). Taken together, our results demonstrate the ability of the Cdc42 sensors to specifically detect activated Cdc42 in vivo.

Measurement of FRET in Living Cells Using GEF Sensors. Transiently transfected NIH 3T3 cells were used to measure the ability of the L198K GEF sensor, the best one in vitro, to monitor GEF activity in vivo. As before, cells were transfected with sensor and various signaling molecules. In cells transfected only with sensor, the average FRET value is 1.61 (Figures 5B and 6C). In cells cotransfected with GEF sensor and SopE, FRET decreases to 1.13 (Figures 5B and 6C). Continuing the trend observed with the Cdc42 sensors, the L198K GEF sensor gives a 1.7-fold reduction in FRET emission ratio in vitro but only a 1.4-fold reduction in vivo. Based on the uniform brightness of transfected cells, the GEF sensor is evenly distributed throughout the cells either when transfected alone or together with SopE. As a control, cells transfected with GEF sensor and YopE display no significant decreases in FRET (Figures 5B and 6C) (*46*, *51*). Thus, the GEF sensor is able to specifically report on Cdc42 exchange activity in vivo and will be useful for complementing and extending the studies conducted with the Cdc42 sensors described above.

DISCUSSION

In this study, we sought to develop genetically encoded sensors that would specifically detect Cdc42 activity in vivo using intramolecular FRET. The sensors described here will report directly on the Cdc42 pathway, without interference from Rac, because they are based on the GBD regions of WASP and N-WASP, specific effectors of Cdc42. The successful creation of Cdc42 and Cdc42-GEF sensors stems directly from our detailed understanding of the biophysical and biochemical characteristics of the Cdc42−WASP interaction. These structural insights allowed us not only to develop sensors based on the GBD of WASP but also to create molecules encompassing a larger region of WASP, the GBD-VCA, which we correctly hypothesized would undergo even larger FRET changes than the GBD alone.

There are a number of potential pitfalls associated with FRET-based imaging technologies that we have attempted to overcome in our design strategy (*27*). Whenever analyzing a FRET signal, one must ascertain that confounding factors, such as donor bleedthrough and direct acceptor emission, are not producing artificial results. Some GTPase sensors have been developed that utilize FRET-paired fluorophore-tagged GTPases together with fluorophore-tagged GBDs (*23*−*25*, *52*). These bimolecular strategies require proper accounting of relative donor and acceptor concentrations, since artifactual FRET changes can be observed if these are not uniform throughout the cell over the course of the experiment. By incorporating our FRET-paired fluorophores into a single molecule, we have simplified the analysis and quantitation of our FRET data (*27*). Some bimolecular FRET studies have employed microinjection of one or both fluorescent partners, which limits their possible range of applications. These studies also do not have the potential to monitor endogenous GTPase activity because the protein being studied must be fluorescently labeled. Our sensors are genetically encoded and can be easily delivered into many different cellular systems. With improved sensitivity they have the potential to monitor endogenous Cdc42. In addition, sensor-expressing stable cell lines can be generated. These benefits will afford a wide range of biological applications. These design considerations could also facilitate high-throughput screens for molecules able to modulate Cdc42 signaling in vivo, to control processes such as tumor metastasis (*53*).

Recently, single-molecule sensors for Ras and Rap1 GEFs were reported, with a molecular construction analogous to

our Cdc42 GEF sensors. Biochemical characteristics of the Ras and Rap1 GEF sensor responses to GEFs and GAPs have not been reported. However, on the basis of our Cdc42 GEF sensor results, it is likely that these molecules, like ours, will respond to GAP proteins with slower kinetics than wild-type GTPases. Sensors of this class may primarily be useful for monitoring the kinetics of GTPase activation and may be more limited for studying processes requiring rapid GTP turnover. These limitations highlight the importance of development and utilization of complementary probes (e.g., sensors for both Cdc42 and Cdc42 GEF) to allow timing issues to be more accurately studied.

Using the FRET-based biosensors reported here, it should be possible to obtain detailed spatial and temporal information on Cdc42 responses evoked by various stimuli. Our current experimental conditions did not allow direct observation of endogenous Cdc42 activation, and activity could only be detected in cells supplemented with Cdc42. In our model in vivo system, we have observed a relatively uniform activation of Cdc42 throughout the cell by exchange factors. This uniform activation is likely due to the high levels of Cdc42 found in these cells, and an important future goal is to determine how the pattern of Cdc42 activation differs in cells expressing endogenous levels of GTPase. It is possible that endogenous Cdc42 activity is not observed in our model system because the relative concentration of sensor to Cdc42 is too high, which results in a high background level of unbound sensor even under maximal activation.

To suppress this background noise, either Cdc42 will have to be expressed ectopically, thereby artificially increasing its cellular concentration, or the sensors will have to be produced at much lower concentrations in the cell. Since the goal of these studies is to study endogenous signaling pathways, our efforts are focused on achieving the latter by creating low-expression-level cell lines. Another consideration is that active Cdc42 is membrane-localized, while inactive Cdc42 is sequestered in the cytosol by RhoGDI (*13*). It is not clear how interaction with RhoGDI affects the ability of the sensors to detect GTPase activity, but membrane targeting of the sensors could likely eliminate the confounding observation of GDI complexes. Membrane localization will also increase the sensitivity of the sensors by localizing them to the sites of Cdc42 action. However, Cdc42 must transit several distinct types of membrane systems, such as Golgi, plasma, and vesicular membranes, to carry out its many varied functions (*54*). The specific membrane-targeting signal used to control sensor localization may bias the membrane distribution of the sensor and may only allow a subset of Cdc42-dependent processes to be observed. This could be overcome by using different targeting sequences for different applications. Evanescent wave microscopy, a particularly sensitive technique for observing events proximal to the plasma membrane, may also prove useful for studying aspects of Cdc42 biology. It is unlikely that any single sensor system will address all the complexities associated with Cdc42. Therefore, to optimally study GTPase signaling in vivo, we will likely require the use of several complementary reagents, methods, and technologies. Several possible strategies have been described above, and implementing these devices is an important goal for the future.

Thus far, we have created a series of Cdc42 sensors varying 100-fold in terms of their affinity for active Cdc42. Consistent with a sequestration model of VCA activation, the GBD-only sensors have higher affinities for active Cdc42, while the GBD-VCA sensors possess the highest FRET ratio changes. Theoretically, both the high-affinity and the high-ratio sensors should be of value in further in vivo studies. In applications where sensitivity is an issue, the high-affinity sensors should enable us to detect activation of relatively low amounts of Cdc42. In other instances, the high-ratio sensors should serve to more finely describe the range of Cdc42 activation levels that can be achieved in the cell. Thus, not only will the sensors be used to determine the spatial and temporal characteristics of Cdc42 activation in response to various stimuli but they could also be used for quantitatively analyzing the amount of Cdc42 that becomes activated by each stimulus. By comparing and contrasting the activation profile of Cdc42 in response to various stimuli, it might be possible to understand the molecular basis for the pleiotropic cellular actions of Cdc42.

Our results show that the Cdc42 and Cdc42 GEF sensors are both faithful reporters of Cdc42 signaling pathways in vivo. We have established the feasibility of using these sensors for studying the real-time dynamics of endogenous Cdc42 in living cells. By using both sensors in parallel studies to monitor consecutive steps in a specific signaling cascade, we will have an internal control for our results since both reporters should agree in terms of the cellular localization and timing of Cdc42 activation. In addition, by comparing GEF activity with Cdc42 activity, we may be able to learn how much GEF signal actually reaches Cdc42 and how much is expended as cellular noise. These issues are at the heart of understanding the efficiency, fidelity, and proper regulation of cellular signal transduction.

ACKNOWLEDGMENT

We thank Rashu Bhargava Seth, Vivek K. Arora, Eduardo Torres, and Dr. Masaya Yamamoto for helpful discussions. We also thank Dr. Gaya K. Amarasinghe and Daisy W. Leung for critical reading of the manuscript.

REFERENCES

1. Pawson, T., and Scott, J. D. (1997) *Science 278*, 2075−2080.
2. Teruel, M. N., and Meyer, T. (2000) *Cell 103*, 181−184.
3. Van Aelst, L., and D'Souza-Schorey, C. (1997) *Genes Dev. 11*, 2295−2322.
4. Hall, A. (1998) *Science 279*, 509−514.
5. Scheffzek, K., Ahmadian, M. R., and Wittinghofer, A. (1998) *Trends Biochem. Sci. 23*, 257−262.
6. Zheng, Y. (2001) *Trends Biochem. Sci. 26*, 724−732.
7. Erickson, J. W., and Cerione, R. A. (2001) *Curr. Opin. Cell Biol. 13*, 153−157.
8. Bishop, A. L., and Hall, A. (2000) *Biochem. J. 348* (Part 2), 241−255.
9. Aspenstrom, P. (1999) *Curr. Opin. Cell Biol. 11*, 95−102.
10. del Pozo, M. A., Price, L. S., Alderson, N. B., Ren, X. D., and Schwartz, M. A. (2000) *EMBO J. 19*, 2008−2014.
11. Cannon, J. L., Labno, C. M., Bosco, G., Seth, A., McGavin, M. H., Siminovitch, K. A., Rosen, M. K., and Burkhardt, J. K. (2001) *Immunity 15*, 249−259.
12. Chiu, V. K., Bivona, T., Hach, A., Sajous, J. B., Silletti, J., Wiener, H., Johnson, R. L., Cox, A. D., and Philips, M. R. (2002) *Nat. Cell Biol. 4*, 343−350.
13. Symons, M., and Settleman, J. (2000) *Trends Cell Biol. 10*, 415−419.
14. Erickson, J. W., Zhang, C., Kahn, R. A., Evans, T., and Cerione, R. A. (1996) *J. Biol. Chem. 271*, 26850−26854.
15. Kroschewski, R., Hall, A., and Mellman, I. (1999) *Nat. Cell Biol. 1*, 8−13.

16. Michaelson, D., Silletti, J., Murphy, G., D'Eustachio, P., Rush, M., and Philips, M. R. (2001) *J. Cell Biol. 152*, 111−126.
17. Linder, S., Nelson, D., Weiss, M., and Aepfelbacher, M. (1999) *Proc. Natl. Acad. Sci. U.S.A. 96*, 9648−9653.
18. Caron, E., and Hall, A. (1998) *Science 282*, 1717−1721.
19. Nobes, C. D., and Hall, A. (1999) *J. Cell Biol. 144*, 1235−1244.
20. Etienne-Manneville, S., and Hall, A. (2001) *Cell 106*, 489−498.
21. Benard, V., Bohl, B. P., and Bokoch, G. M. (1999) *J. Biol. Chem. 274*, 13198−13204.
22. Kim, S. H., Li, Z., and Sacks, D. B. (2000) *J. Biol. Chem. 275*, 36999−37005.
23. Kraynov, V. S., Chamberlain, C., Bokoch, G. M., Schwartz, M. A., Slabaugh, S., and Hahn, K. M. (2000) *Science 290*, 333−337.
24. Del Pozo, M. A., Kiosses, W. B., Alderson, N. B., Meller, N., Hahn, K. M., and Schwartz, M. A. (2002) *Nat. Cell Biol. 4*, 232−239.
25. Katsumi, A., Milanini, J., Kiosses, W. B., Del Pozo, M. A., Kaunas, R., Chien, S., Hahn, K. M., and Schwartz, M. A. (2002) *J. Cell Biol. 158*, 153−164.
26. Mochizuki, N., Yamashita, S., Kurokawa, K., Ohba, Y., Nagai, T., Miyawaki, A., and Matsuda, M. (2001) *Nature 411*, 1065−1068.
27. Gordon, G. W., Berry, G., Liang, X. H., Levine, B., and Herman, B. (1998) *Biophys. J. 74*, 2702−2713.
28. Miyawaki, A., Griesbeck, O., Heim, R., and Tsien, R. Y. (1999) *Proc. Natl. Acad. Sci. U.S.A. 96*, 2135−2140.
29. Kim, A. S., Kakalis, L. T., Abdul-Manan, N., Liu, G. A., and Rosen, M. K. (2000) *Nature 404*, 151−158.
30. Buck, M., Xu, W., and Rosen, M. K. (2001) *Biochemistry 40*, 14115−14122.
31. Abdul-Manan, N., Aghazadeh, B., Liu, G. A., Majumdar, A., Ouerfelli, O., Siminovitch, K. A., and Rosen, M. K. (1999) *Nature 399*, 379−383.
32. Rossman, K. L., Worthylake, D. K., Snyder, J. T., Siderovski, D. P., Campbell, S. L., and Sondek, J. (2002) *EMBO J. 21*, 1315−1326.
33. Hardt, W. D., Chen, L. M., Schuebel, K. E., Bustelo, X. R., and Galan, J. E. (1998) *Cell 93*, 815−826.
34. Zheng, Y., Fischer, D. J., Santos, M. F., Tigyi, G., Pasteris, N. G., Gorski, J. L., and Xu, Y. (1996) *J. Biol. Chem. 271*, 33169−33172.
35. Zigmond, S. H. (2000) *J. Cell Biol. 150*, 117−120.
36. Higgs, H. N., and Pollard, T. D. (1999) *J. Biol. Chem. 274*, 32531−32534.
37. Thompson, G., Owen, D., Chalk, P. A., and Lowe, P. N. (1998) *Biochemistry 37*, 7885−7891.
38. Rudolph, M. G., Bayer, P., Abo, A., Kuhlmann, J., Vetter, I. R., and Wittinghofer, A. (1998) *J. Biol. Chem. 273*, 18067−18076.
39. Lei, M., Lu, W., Meng, W., Parrini, M. C., Eck, M. J., Mayer, B. J., and Harrison, S. C. (2000) *Cell 102*, 387−397.
40. Mott, H. R., Owen, D., Nietlispach, D., Lowe, P. N., Manser, E., Lim, L., and Laue, E. D. (1999) *Nature 399*, 384−388.
41. Miyawaki, A., and Tsien, R. Y. (2000) *Methods Enzymol. 327*, 472−500.
42. Miki, H., Sasaki, T., Takai, Y., and Takenawa, T. (1998) *Nature 391*, 93−96.
43. Rudolph, M. G., Linnemann, T., Grunewald, P., Wittinghofer, A., Vetter, I. R., and Herrmann, C. (2001) *J. Biol. Chem. 276*, 23914−23921.
44. Morreale, A., Venkatesan, M., Mott, H. R., Owen, D., Nietlispach, D., Lowe, P. N., and Laue, E. D. (2000) *Nat. Struct. Biol. 7*, 384−388.
45. Owen, D., Mott, H. R., Laue, E. D., and Lowe, P. N. (2000) *Biochemistry 39*, 1243−1250.
46. Von Pawel-Rammingen, U., Telepnev, M. V., Schmidt, G., Aktories, K., Wolf-Watz, H., and Rosqvist, R. (2000) *Mol. Microbiol. 36*, 737−748.
47. Leonard, D. A., Evans, T., Hart, M., Cerione, R. A., and Manor, D. (1994) *Biochemistry 33*, 12323−12328.
48. Nassar, N., Hoffman, G. R., Manor, D., Clardy, J. C., and Cerione, R. A. (1998) *Nat. Struct. Biol. 5*, 1047−1052.
49. Rittinger, K., Walker, P. A., Eccleston, J. F., Nurmahomed, K., Owen, D., Laue, E., Gamblin, S. J., and Smerdon, S. J. (1997) *Nature 388*, 693−697.
50. Feig, L. A. (1999) *Nat. Cell Biol. 1*, E25−E27.
51. Fu, Y., and Galan, J. E. (1999) *Nature 401*, 293−297.
52. Plafker, K. S., and Macara, I. G. (2002) *J. Biol. Chem.* (in press).
53. Boettner, B., and Van Aelst, L. (2002) *Gene 286*, 155−174.
54. Ridley, A. J. (2001) *Traffic 2*, 303−310.
55. Carson, M. J. (1991) *J. Appl. Crystallogr. 24*, 958−961.

BI026881Z